Applied Catalysis A: General 435–436 (2012) 93–98

Contents lists available at SciVerse ScienceDirect

Applied Catalysis A: General

journal homepage: www.elsevier.com/locate/apcata

Photocatalytic and photoelectrochemical properties of in situ carbon hybridized $BiPO_4$ films

Bin Lu[a,b], Xinguo Ma[a], Chengsi Pan[a], Yongfa Zhu[a,*]

[a] Department of Chemistry, Tsinghua University, Beijing 100084, PR China
[b] Shanghai Municipal Engineering Design Institute, Shanghai 200092, PR China

ARTICLE INFO

Article history:
Received 17 March 2012
Received in revised form 25 May 2012
Accepted 26 May 2012
Available online 4 June 2012

Keywords:
$BiPO_4$
Carbon
Hybridization
Photo-induced carriers separation

ABSTRACT

In situ hybridization of carbon with $BiPO_4$ films were performed through calcination of amorphous complex precursor films on the Ti substrate under various temperatures. The $BiPO_4$ crystallites were in situ grown into $BiPO_4$ particles on the surface of the Ti substrate. The formed $BiPO_4$ particles in situ hybridized with the residual carbon from precursor calcination to form carbon hybridized $BiPO_4$ films. The extent of hybridization depended on the calcination temperatures. The photocatalytic activities of carbon hybridized $BiPO_4$ films under different calcination temperatures were estimated through photocatalytic degradation of methylene blue. The results indicated that the film prepared at 400 °C presented the highest photocatalytic activity, which was about 1.5 times than that of the film at 550 °C. This phenomenon could be attributed to the higher carbon hybridization extent, higher transfer efficiency of photo-induced electrons between carbon and $BiPO_4$ crystalline nanoparticles in films, and corresponding separation efficiency of photo-induced electrons and holes. The electronic interaction was also systematically investigated by the photoelectrochemical measurements.

1. Introduction

In recent years, photocatalytic processes have been intensively paid attention as a promising advanced oxidation technology used for environmental remediation [1,2]. Among photocatalysts, TiO_2 has been paid more attention for its ability of complete degradation of recalcitrant organic pollutants [3–5]. But the photocatalytic oxidation activity of TiO_2 is not high enough to meet the demand of industrial practice due to a rapid recombination between photo-induced electrons and holes [6,7]. Although more new photocatalysts, mostly focused on metal oxide and composite metal oxide [8–10], have been estimated in the past, the efficient photocatalysts with high photocatalytic activity, good stability, and low cost are still in lack. More recently, the nonmetal oxy-acid salt photocatalysts have been reported to be effective to enhance the photocatalytic activity [11,12]. As these nonmetal oxy-acid salt photocatalysts, $BiPO_4$ with space group of $P21/n$ was firstly reported by our research group to have the higher photocatalytic activity than $P25$ under UV irradiation [11]. The enhanced photocatalytic activity was suggested to be the results of the high negative energy of nonmetal anion groups to draw the hole to the interface by electrostatic force and the chemical redox inertness to the photogenerated electrons and holes. There also exists another $BiPO_4$ crystal phase with the space group of $P21/m$. But, the photocatalytic activity of $BiPO_4$ with $P21/m$ was not reported clear. Herein, the $BiPO_4$ films with the space group of $P21/m$ were prepared and estimated on their photocatalytic activities. In order to enhance the photocatalytic activity of the given photocatalysts, much attention has been focused on the recombination inhibition of photo-induced electrons and holes by coupling other materials. These required materials could induce higher transfer efficiency for photo-induced carriers, typical those materials such as noble metals [13,14] and semiconductors [15,16]. Our research group has also developed a series of conjugative structure material, such as C_{60} [6,7], polyaniline [17,18], which could hybridize with semiconductor for enhanced photocatalytic activity. Recently, some efforts have been made to utilize the unique properties of carbon to increase the efficiency of photocatalysis [19]. However, the interior mechanism and some details are yet not very clear. In this study, residual carbon was in situ prepared and hybridized with $BiPO_4$ crystalline particles to form carbon hybridized $BiPO_4$ films. It is expected that the hybridization of photocatalyst with carbon would reduce the recombination of photo-induced electrons and holes and increase the photocatalytic activity. Enormous enhancement of photocatalytic activity was observed on the prepared carbon hybridized $BiPO_4$ films. The structure and interface electronic interaction between carbon and $BiPO_4$ crystalline particles in films, as well as the resulting effect on the photocatalytic activity were also systematically investigated.

* Corresponding author. Tel.: +86 010 6278 3586; fax: +86 010 6278 7601.
E-mail address: Zhuyf@mail.tsinghua.edu.cn (Y. Zhu).

0926-860X/$ – see front matter © 2012 Elsevier B.V. All rights reserved.
http://dx.doi.org/10.1016/j.apcata.2012.05.043

Table 1
Average size of crystalline grains and thickness of $BiPO_4$ films under various calcination temperatures.

Calcination temperature (°C)	Average size of crystalline grains of (0 2 0) plane (nm)	Thickness of films (nm)
400	118	170
450	150	175
500	189	191
550	222	192

2. Experimental

2.1. Preparation of the $BiPO_4$ film

Titanium foil (thickness about 250 μm, purity 99.4%, Beijing Cuibolin Non-Ferrous Technology Developing Co. Ltd.) was chemically polished before it was used as substrate for $BiPO_4$ film deposition. All other chemicals were of analytical grade and used without further purification. Deionized water was used throughout the experiment. Carbon hybridized $BiPO_4$ films deposited on titanium substrate were prepared through calcinating an amorphous complex precursor films in air. The films were prepared via the dip-coating method as follows. 0.02 mol of diethylenetriaminepentaacetic acid (H_2DTPA) as chelating agent for bismuth cation was under fiercely stirring added into 200 mL of 80 °C deionized water. 7.5 mL of ammonia was in sequence added into the above mixture solution to improve hydrolysis of H_2DTPA. When H_2DTPA was completely dissolved, 0.005 mol of Bi_2O_3 and 0.01 mol of $NH_4H_2PO_4$ were added and the yellow suspensions also completely chelated into the clarified solution. The molar ratio of metal ions to H_2DTPA was 1:2. The above solution was dried at 80 °C for 3 days to obtain the required amorphous complex precursor. The precursor solution of 50% concentration was prepared by diluting the above precursor with deionized water. The precursor solution was used as dip-coating solution. Using the dip-coating method, the precursor dissolved in above precursor solution was deposited onto a titanium substrate, and calcined in air under various temperatures for 4 h using a muffle furnace with 3 °C/min of heating rate to form $BiPO_4$ films.

2.2. Characterization of the $BiPO_4$ film

The morphologies of the $BiPO_4$ films were characterized by an S-5500 electron scanning microscope (SEM) with the accelerating voltage of 5.0 kV and emission current of 5.9 μA. X-ray diffraction (XRD) patterns of the $BiPO_4$ films were measured by a Rigaku DMAX-2400 diffractometer with Cu Kα radiation. The average size of $BiPO_4$ crystalline grains was determined from XRD pattern parameters according to the Scherrer equation: $D_c = K\lambda/(\beta \cos\theta)$, where D_c is the average crystallite size, K is the Scherrer constant equal to 0.89, β is the full width at half-maximum (FWHM), and θ is the diffraction angle. The Auger electron spectroscopy (AES) technique was used to determine the thickness of the prepared $BiPO_4$ films. The energy and beam current of the Ar ion beam was 3.0 keV and 6 μA, respectively. The beam diameter was 1 mm and the sputtering rate was approximately 12.0 nm/min. The average size of $BiPO_4$ crystalline grains and the thicknesses of the films under various calcination temperatures are listed in Table 1. Raman spectra were acquired with a Raman microspectrometer (Renishaw 1000NR) using an Ar ion laser (514 nm). Raman spectra were measured under a microscope, using an objective with 20 times magnifier to focus the incident excitation laser radiation into a spot 1–2 or 2–3 μm in diameter to collect the scattered light. Spectra were collected in the range of 2000–100 cm^{-1} with a resolution of 1 cm^{-1}.

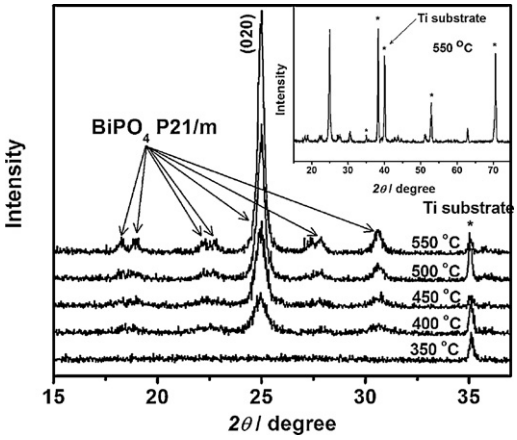

Fig. 1. XRD of the $BiPO_4$ films prepared in air under various calcination temperatures.

2.3. Photoelectrochemical and photocatalytic performance testing

Photoelectrochemical measurement was performed on a CHI660D electrochemical system with a counter electrode (Pt wire, 70 mm in length with a diameter of 0.4 mm), a working electrode ($BiPO_4$ films deposited on a 2 cm × 4 cm titanium foil) and a reference electrode (a saturated calomel electrode, SCE). A quartz electrolytic cell was employed, filled with 100 mL of 0.5 M Na_2SO_4 solution. A 20 W germicidal lamp (~90% of energy output at 253.7 nm) was used as irradiation source. The intensity of light, as measured by an UV-irradiance meter (UV-A, Instruments of Beijing Normal University), was 1.25 mW/cm^2 on the prepared film electrode. Photocatalytic degradation of methylene blue was performed with the initial concentration of 10 μM in 50 mL solution. The concentration of methylene blue was measured using Hitachi U-3010 UV–vis spectrophotometer.

3. Results and discussion

3.1. Crystal phase, morphologies and formation mechanism of the $BiPO_4$ films

The powder X-ray diffraction patterns of the $BiPO_4$ films prepared under various calcination temperatures are shown in Fig. 1. As shown in Fig. 1, the characteristic peaks of $BiPO_4$ with space group of $P21/m$ (JCPDS 77-2208) were observed on the $BiPO_4$ films prepared under the calcination temperatures of 400 °C, 450 °C, 500 °C, and 550 °C at the diffraction angles of 18.28°, 19.03°, 22.26°, 22.78°, 24.99°, 27.95°, and 30.61°. The sample calcined under 350 °C only presented the diffraction patterns of titanium substrate. The diffraction peaks became sharper and sharper and their intensities also gradually increased with increasing calcination temperatures, indicating better crystallinity achieved at higher calcination temperatures. From Table 1, the average size of crystalline grains of (0 2 0) plane gradually grew from 118 nm to 222 nm with increasing calcination temperatures, indicating that the $BiPO_4$ crystalline particles would grow larger and larger at the higher calcination temperature. The thickness of $BiPO_4$ film at 400 °C was similar to that at 450 °C, different from those at 500 °C and 550 °C. This phenomenon could imply that a different geometric structure of $BiPO_4$ films could be formed at 400 °C and 450 °C compared with those at 500 °C and 550 °C. Besides, it is noticeable that only the diffraction peak of (0 2 0) crystal plane at 24.99° was evidently enhanced with increasing calcination temperatures. This phenomenon indicates that the growth of $BiPO_4$ crystalline

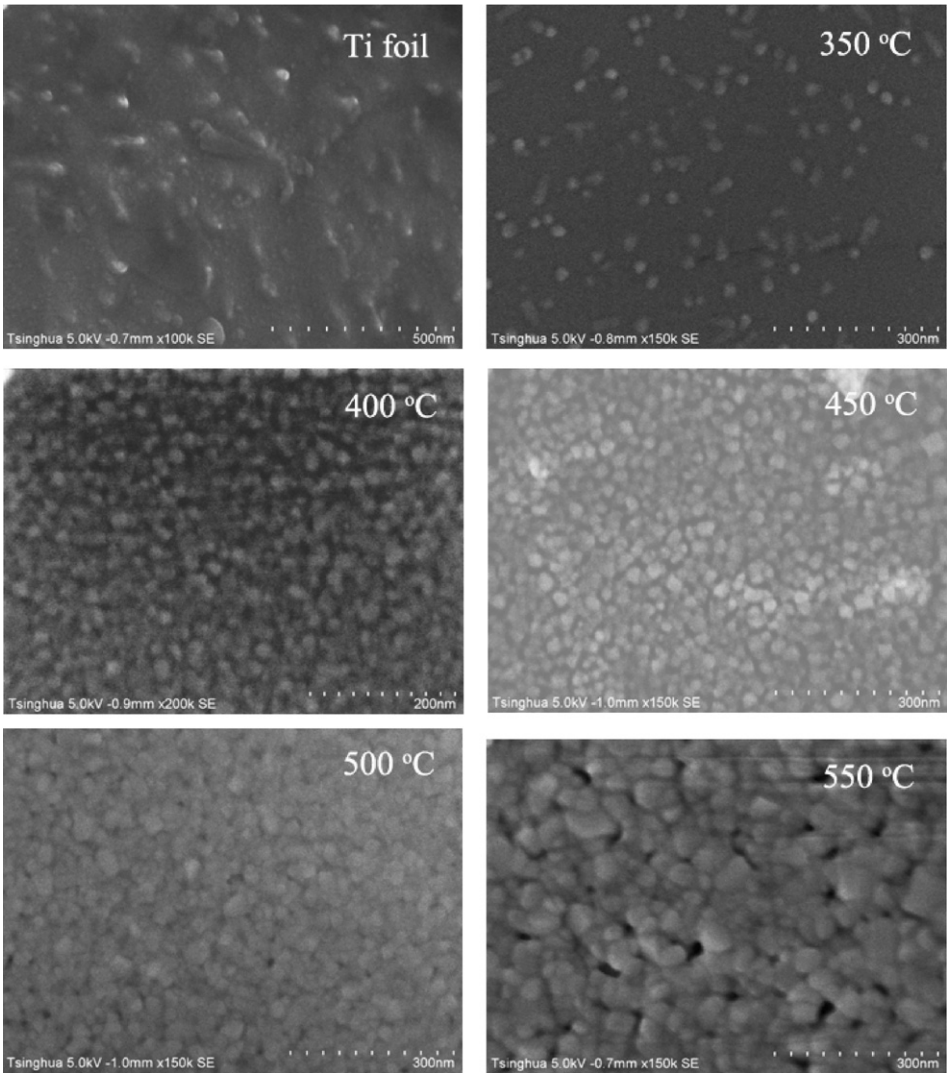

Fig. 2. SEM of the titanium substrate and $BiPO_4$ films prepared in air under various calcination temperatures.

grain on titanium substrate was anisotropic only along the (0 2 0) plane, which could be due to the induction effect of titanium lattice structure. So it is reasonable to say that $BiPO_4$ crystalline grains were firstly formed on the surface of titanium substrate and gradually grew larger and larger when increasing calcination temperatures.

Fig. 2 shows the morphologies of the prepared $BiPO_4$ films under various calcination temperatures. The film treated at 350 °C consisted of sparsely distributed nanoparticles with the size of about 15 nm. At 400 °C and 450 °C, the $BiPO_4$ films were homogeneously composed of thousands of nanoparticles. These nanoparticles was about 30 nm sized. There also existed substantial interstices of 10 nm between these nanoparticles. At 500 °C, nanoparticles grew larger up to about 40–50 nm and overlapped each other. The interstices also disappeared. At 550 °C, the nanoparticles almost completely fused with each other and presented some porous structure. These varieties of morphologies of $BiPO_4$ films are also strongly consistent with that of crystalline grains and thicknesses with increasing calcination temperatures (Table 1).

According to the above results that the crystal lattice of titanium substrate would produce an induction effect on grown (0 2 0) crystal plane of $BiPO_4$ crystalline grains (Fig. 1) and the morphologies of $BiPO_4$ films varies with various calcination temperatures (Fig. 2), the formation mechanism of $BiPO_4$ films can be deduced as followings as shown in Fig. 3. The crystalline grains of $BiPO_4$ could be firstly homogeneously formed on the interface between the precursor film and titanium substrate (Fig. 3(a)), then grow up larger and larger with interstices formed between $BiPO_4$ nanoparticles (Fig. 3(b) and (c)), and finally get completely inosculated into the $BiPO_4$ film with some porous structure (Fig. 3(d)).

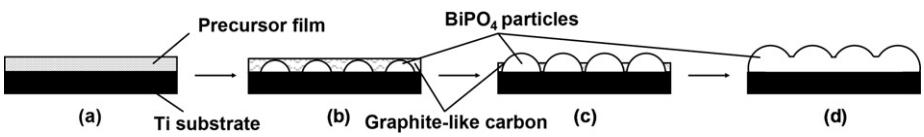

Fig. 3. Schematics of the formation mechanism of $BiPO_4$ films.

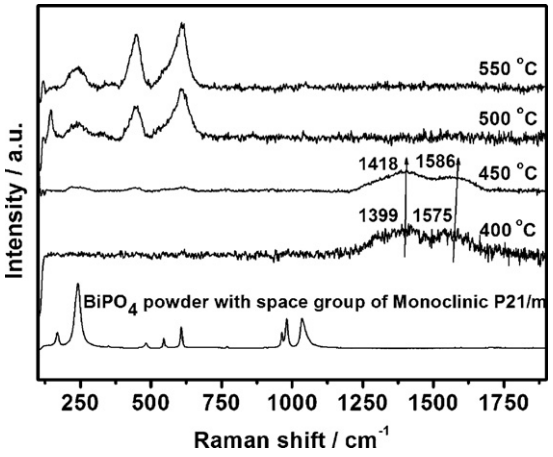

Fig. 4. Raman patterns of the $BiPO_4$ films prepared in air under various calcination temperatures.

3.2. Hybridization structure

Fig. 4 shows the Raman patterns of the $BiPO_4$ films prepared under various calcination temperatures. Two peaks around 1399 and 1575 cm^{-1}, often referenced to be the Raman-active mode of carbon-type structure, were observed to be weakened when increasing the calcination temperatures and completely disappeared at 500 °C and 550 °C. This implied that some carbon-type structure was in situ formed in the $BiPO_4$ films prepared at 400 °C and 450 °C, due to the oxidation of the precursor films containing hydrocarbon compounds. The Raman-active E_{2g} mode at 1575 cm^{-1} is characteristic for Raman-active E_{2g} mode of sp^2-bonded carbon atoms in a two-dimensional hexagonal grapheme layer [20]. The Raman-active E_{2g} mode at 1399 cm^{-1} could be attributed to the presence of defects within the hexagonal graphitic structure. Since the intensities of Raman-active mode at 1575 cm^{-1} are comparable to those at 1399 cm^{-1}, we conclude that the $BiPO_4$ films prepared at 400 °C and 450 °C have some degree of atomic-scale carbon ordering. In addition, Raman peaks around 1399 and 1575 cm^{-1} shifted to higher wavenumbers in the sample prepared at 450 °C, which suggests some structural imperfections of the carbon-type structure.

Mott–Schottky (MS) measurements were performed in darkness by using the impedance technique. Fig. 5 shows MS plots of the prepared $BiPO_4$ films electrodes. All prepared samples are observed reversed sigmoidal plots with an overall shape, which are consistent with that typical for n-type semiconductors. The MS plots of all

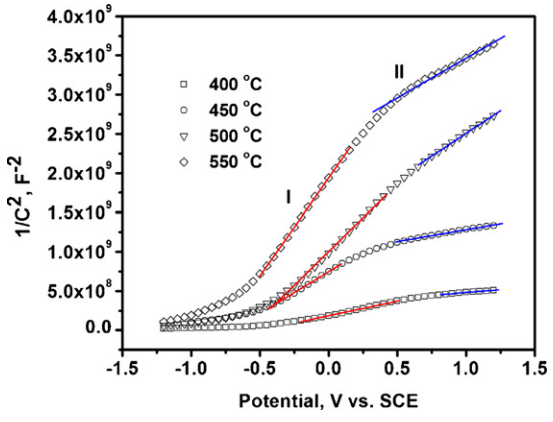

Fig. 5. Mott–Schottky plots in dark of the $BiPO_4$ films prepared in air under various calcination temperatures.

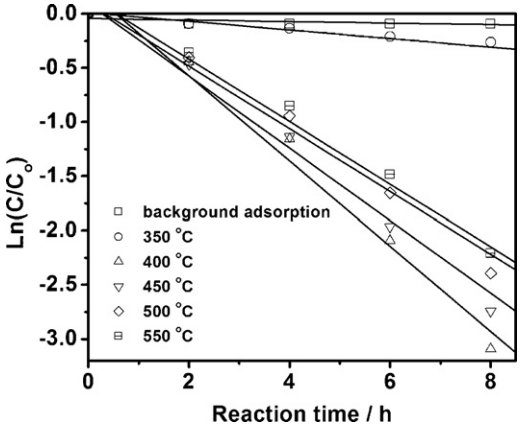

Fig. 6. Photocatalytic degradation of methylene blue by the $BiPO_4$ films prepared at various calcination temperatures.

samples consist of two linear ranges: I from about −0.5 V to 0.5 V vs. SCE and II from about 0.5 V to 1.2 V vs. SCE. The linear range I can be ascribed to the effect of potential on capacitance of depletion layer in the $BiPO_4$ films, which can be interpreted by Eq. (1), where e is the electronic charge, N_A is the density of carbon hybridized, ε_0 is the permittivity of free space, ε is the relative permittivity, V is the applied potential, V_{fb} is the flat band potential, k is the Boltzmann constant, and T is the temperature [21].

$$C^{-2} = \left(\frac{2}{eN_A\varepsilon_0\varepsilon}\right)\left(|V - V_{fb}| - \frac{kT}{e}\right) \quad (1)$$

From this equation, it can be seen that the slopes of linear range I in MS plots are inversely proportional to the density of carbon hybridized. Therefore, $BiPO_4$ films prepared at 400 °C and 450 °C presented more intense hybridization with carbon than those prepared at 500 °C and 550 °C. The linear range II could be ascribed to extension of the depletion layer to the interface between $BiPO_4$ film and titanium substrate when increasing potential [22]. Similarly, the slopes of the prepared films at 400 °C and 450 °C are lower than that of the films prepared at 500 °C and 550 °C. Considering that there exist substantial interstices of 10 nm between the particles in the films at 400 °C and 450 °C and there do not at 500 °C and 550 °C, this result also indicates that carbon would also hybridize with titanium substrate in the films prepared at 400 °C and 450 °C.

3.3. Photocatalytic and photoelectrochemical properties

Fig. 6 shows the effect of calcination temperatures on photocatalytic activities of the prepared $BiPO_4$ films. Typically, the highest photocatalytic activity was observed in the $BiPO_4$ film prepared at 400 °C, whose reaction rate is 1.5 times higher than that in the film prepared at 550 °C. This implies that there exist some synergistic effects induced by in situ carbon hybridization of $BiPO_4$ film for enhanced photocatalytic activity.

The stable photocurrent and transition photocurrent measurements were carried out for the $BiPO_4$ films prepared at various calcination temperatures (Fig. 7). The potential of the working electrode against Pt counter electrode was set at open circuit potential. A stable anodic photocurrent is observed for each switch-on and switch-off event in all prepared $BiPO_4$ film electrodes (Fig. 7(a)). This photo-responsive phenomenon is entirely reversible. The stable photocurrent of the film prepared at 400 °C is 3.6 times higher than that of the film prepared at 550 °C, which indicates that the stronger oxidation potential is obtained by in situ hybridization of carbon with $BiPO_4$ film. The separation efficiency of photo-induced electrons and holes is improved through the electronic interaction between carbon and $BiPO_4$ crystalline particles formed in the film.

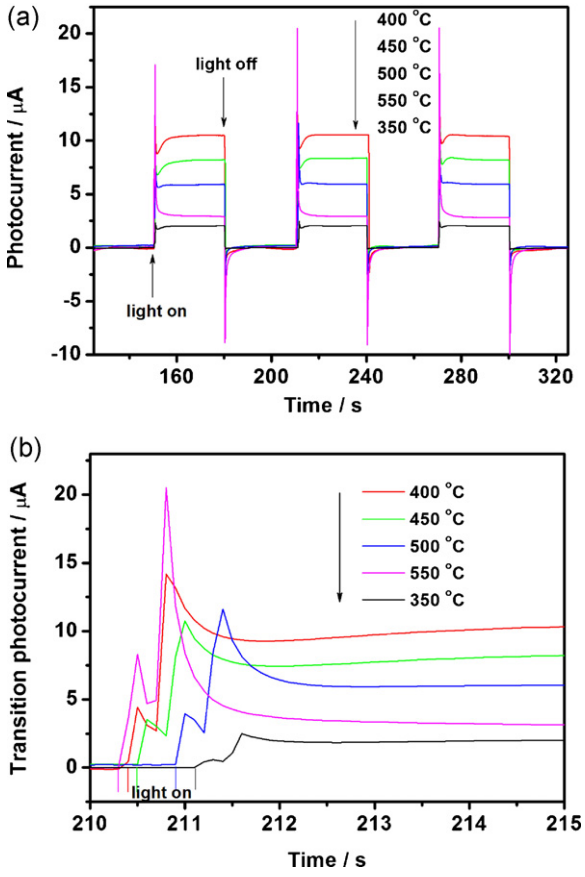

Fig. 7. The stable photocurrent (a) and transition photocurrent (b) of the $BiPO_4$ films prepared at various temperatures.

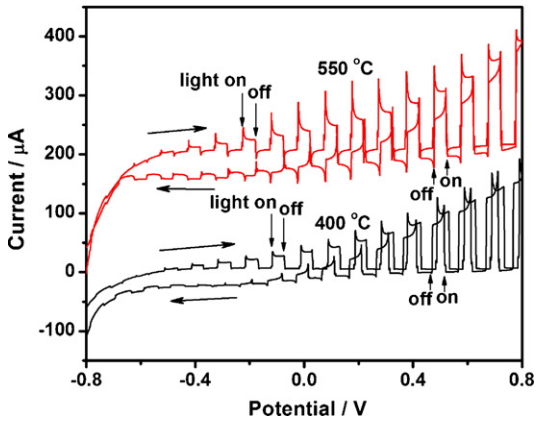

Fig. 8. Cyclic voltammograms during chopped UV irradiation excitation of the $BiPO_4$ films prepared at 400 and 550 °C.

In addition, the initial anodic photocurrent spike and its subsequent decay as observed in Fig. 7(b) are a typical indication of surface recombination [23,24]. The decay range of initial anodic photocurrent spike in the film prepared at 400 °C is from 14 μA of the peak photocurrent to 9 μA of stable photocurrent, which is much smaller than that of the film prepared at 550 °C is from 21 μA of the peak photocurrent to 3.5 μA of stable photocurrent. This indicates that the slower recombination of photo-induced electrons and holes is observed with in situ hybridization of carbon with $BiPO_4$ film. It is consistent with the results from their stable photocurrent measurements and photocatalytic activities.

Fig. 8 shows the cyclic voltammograms during chopped UV irradiation excitation of the $BiPO_4$ films prepared at 400 °C and 550 °C. From Fig. 8, the onset potential of anodic photocurrent was around −0.52 V vs. SCE in the $BiPO_4$ film prepared at 400 °C when sweeping the potential from the negative to positive direction. The forward anodic photocurrent linearly increased with increasing potential, which presents an n-type semiconductor behavior: electrons migrate to titanium substrate and holes oxidize water. Upon reversing the potential sweeping from the positive to negative direction, the backward anodic photocurrent became slightly lower than forward anodic photocurrent, also linearly decreased with decreasing potential, and turned into a weak cathodic photocurrent at about −0.3 V vs. SCE. The $BiPO_4$ film prepared at 550 °C presented a similar sweeping process on cyclic voltammogram. However, upon reversing the potential from the positive to negative direction, the backward anodic photocurrent of the film at 550 °C was much more reduced compared with that of the films at 400 °C. This phenomenon could be rationalized as formation of surface peroxo species [25] or effect of adsorbed O_2 [26], both serving as electron scavengers. From the positive to negative potential sweeping, these species with oxidation potential could be formed by photo-induced holes on the surface of $BiPO_4$ films when light was turned on. Simultaneously, photo-induced electrons migrate to the titanium to present anodic photocurrent. On the next light on at the lower potential, these formed species could also scavenge the photo-induced electrons to reduce the response of anodic photocurrent and even present the cathodic photocurrent, compared with the forward anodic photocurrent. At the negative potential, adsorbed oxygen or peroxo intermediates would be removed, and therefore no more cathodic photocurrent can be generated. Therefore, these peroxo intermediates or adsorbed O_2 contribute to the undesired back reaction. This also implies that in situ carbon hybridized $BiPO_4$ film may also efficiently inhibit the undesired back reaction.

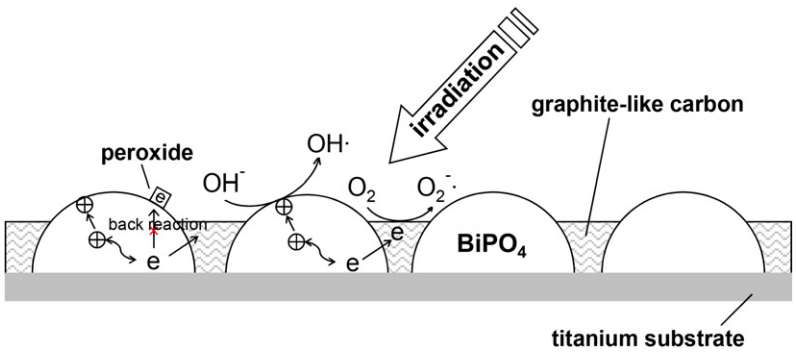

Fig. 9. Schematic drawing of in situ carbon hybridized $BiPO_4$ film.

3.4. Mechanism of photocatalytic activity enhancement

Based on the above results, the electronic interaction between graphite-like carbon and $BiPO_4$ films is confirmed and the enhanced photocatalytic activity can be explained in the following way: Photo-induced electrons and holes with the $BiPO_4$ nanoparticles in the films either take part in redox reactions at the surface, or recombine. The undesired back reaction could also make intermediate peroxo species produced by photo-induced holes scavenge photo-induced electrons. The recombination process and back reaction have a faster kinetics than the redox reactions and therefore controls the efficiency of the photocatalytic process [27]. In the presence of graphite-like carbon, photo-induced electrons are scavenged by graphite-like carbon. Thus, the possibilities of the recombination of electron/hole pairs and scavenging of electron by intermediate peroxo species decrease. Meanwhile, O_2 adsorbed on the surface of the graphite-like carbon can accept electron and form $^{\bullet}O_2^-$ which then oxidizes methylene blue directly on the surface. This mechanism of the enhancement of the photocatalytic activity is illustrated in Fig. 9.

4. Conclusions

The mediating role of carbon in storing and shuttling photo-induced electrons from the semiconductor to an acceptor in a photocatalytic process is realized by hybridizing carbon with $BiPO_4$ crystalline particles in the prepared films. The electronic contact between semiconductor and carbon results in an efficient separation of electron–hole pairs and an effective inhibition of undesired back reaction induced by surface peroxo intermediates, which both minimize the energy-dissipating by electron–hole recombination and undesired back reaction, and subsequently leads to higher photocatalytic activity under UV irradiation.

Acknowledgements

This work is supported by Chinese National Science Foundation (20925725 and 50972070) and National Basic Research Program of China (2007CB613303) and China Postdoctoral Science Foundation (20100480018) for their financial support.

References

[1] J.H. Pan, H. Dou, Z. Xiong, C.X.J. Ma, X.S. Zhao, J. Mater. Chem. 20 (2010) 4512–4528.
[2] N.M. Chong, B. Jim, C.K.W. Chow, C. Saint, Water Res. 44 (2010) 2997–3027.
[3] U.I. Gaya, A.H. Abdullah, Z. Zainal, M.Z. Hussein, J. Hazard. Mater. 168 (2009) 57–63.
[4] F. Han, V.S.R. Kambala, M. Srinivasan, D. Rajarathnam, Appl. Catal. A: Gen. 359 (2009) 25–40.
[5] R. Poblete, E. Otal, L.F. Vilches, J. Vale, C. Fernandez-pereira, Appl. Catal. B: Environ. 102 (2011) 172–179.
[6] J. Lin, R. Zong, M. Zhou, Y. Zhu, Appl. Catal. B: Environ. 89 (2009) 425–431.
[7] L. Zhang, Y. Wang, T. Xu, S. Zhu, Y. Zhu, J. Mol. Catal. A: Chem. 331 (2010) 7–14.
[8] D.W. Hwang, H.G. Kim, J. Kim, K.Y. Cha, Y.G. Kim, J.S. Lee, J. Catal. 193 (2000) 40–48.
[9] C.T.K. Thaminimulla, T. Takata, M. Hara, J.N. Kondo, K. Domen, J. Catal. 196 (2000) 362–365.
[10] A. Kudo, Y. Miseki, Chem. Soc. Rev. 38 (2009) 253–278.
[11] C. Pan, Y. Zhu, Environ. Sci. Technol. 44 (2010) 5570–5574.
[12] Z. Yi, J. Ye, N. Kikugawa, T. Kako, S. Ouyang, H. Stuart-Williams, H. Yang, J. Cao, W. Luo, Z. Li, Y. Liu, R.L. Withers, Nat. Mater. 9 (2010) 559–564.
[13] A. Iwase, H. Kato, A. Kudo, Catal. Lett. 108 (2006) 7–10.
[14] M. Liu, W. You, Z. Lei, G. Zhou, J. Yang, G. Wu, G. Ma, G. Luan, T. Takata, M. Hara, K. Domen, C. Li, Chem. Commun. 19 (2004) 2192–2193.
[15] D. Wang, Z. Zou, J. Ye, Chem. Mater. 17 (2005) 3255–3261.
[16] L. Amirav, A.P. Alivisatos, J. Phys. Chem. Lett. 1 (2010) 1051–1054.
[17] H. Zhang, R. Zong, J. Zhao, Y. Zhu, Environ. Sci. Technol. 42 (2008) 3803–3807.
[18] H. Zhang, R. Zong, Y. Zhu, J. Phys. Chem. C 113 (2009) 4605–4611.
[19] L. Zhang, H. Fu, Y. Zhu, Adv. Funct. Mater. 18 (2008) 2180–2189.
[20] P.C. Eklund, J.M. Holden, R.A. Jishi, Carbon 33 (7) (1995) 959–972.
[21] K. Tse, B.M. Nichols, W. Yang, J.E. Butler, J.N. Russell, R.J. Hamers, J. Phys. Chem. B 109 (2005) 8523–8532.
[22] R. Krol, A. Goossens, J. Schoonman, J. Electrochem. Soc. 144 (1997) 1723–1727.
[23] L.M. Peter, Chem. Rev. 90 (1990) 753–769.
[24] M. Long, W. Cai, H. Kisch, J. Phys. Chem. C 112 (2008) 548–554.
[25] M. Ulmann, R.N. Tacconi, J. Augustynski, J. Phys. Chem. 90 (1986) 6523–6530.
[26] B. Neumann, P. Bogdanoff, H. Tributsch, S. Sakthivel, H. Kisch, J. Phys. Chem. B 109 (2005) 16579–16586.
[27] M.R. Hoffmann, S.T. Martin, W.Y. Choi, D.W. Bahnemann, Chem. Rev. 95 (1995) 69–96.